Iranian (Iranica) Journal of Energy & Environment
Journal Homepage: www.ijee.net
IJEE an official peer review journal of Babol Noshirvani University of Technology, ISSN:2079-2115

Design and Simulation of Air-Solar Preheating Unit: An Improved Design of a Flat Plate Solar Collector

S. N. Nnamchi[1]*, O. A. Nnamchi[2], E. O. Sangotayo[1], S. A. Ismael[1], O. K. Nkurunziza[1], V. Gabriel[3]

[1] *Department of Mechanical Engineering, School of Engineering and Applied Sciences, Kampala International University, Kampala, Uganda*
[2] *Department of Agricultural Engineering and Bio Resources, Michael Okpara University of Agriculture, Umuahia, Nigeria*
[3] *Department of Electrical/Telecommunication/Computer Engineering, SEAS, Kampala International University, Kampala, Uganda*

P A P E R I N F O

Paper history:
Received 06 April 2020
Accepted in revised form 08 June 2020

Keywords:
Air Solar Preheating Unit
Efficiency
Multiple Input Output Design
Optimum Design
Simulation
Solar Energy

A B S T R A C T

The design of a flat-plate solar collector (FPSC) is accomplished by multiple input multiple output (MIMO) design technique. The design variables (absorber, fluid and glass temperatures; length, width, height of the FPSC) were the unknown variables in the commensurate thermal balance equations based on; component, overall and yardstick thermal balance on the FPSC. Then, simulator matrices were setup comprising of coefficient and column matrices of design functions. The elements of the coefficient matrix were the partial derivatives of the design functions with respect to the design variables. Besides the convective and radiative heat transfer coefficients were function of the design variables. The initial values of the design variables (307K, 334.5K, 368K, 2 m, 1 m, and 0.045m, respectively) were set, at the seventh iteration, the output variables (306.9K, 339.15K, 368.1K, 2.01m, 1.005m, 0.04m, respectively) merged as the design functions $\rightarrow 0$ with insignificant change in the design variables. The output results were used to simulate FPSC, to track its responses to changes in the physical conditions, the stimulation revealed some constraints in the design of the FPSC, which is vital information for the overall optimization of the FPSC. The design yardsticks; the thermal efficiency (0.76) and the effectiveness (0.4) are quite pragmatic. This shows that MIMO technique to thermal system design is effective as convergence among the design variables was sought. Moreover, MIMO considered all thermal losses instead of basing the yardsticks on top loss overall transfer coefficient alone; thus, neglecting sidewalls and base losses. Moreover, the advent of connecting box prepares the preheating unit for high temperature drying (> 150 ^{o}C) on integration with a reheating unit.

***doi**: 10.5829/ijee.2020.11.02.02*

INTRODUCTION

The general design approach for the preheating unit (flat-plate solar collector, FPSC and connecting box); is to consider the insulation (solar irradiance) reaching the FPSC and the thermal losses. The net power is equivalent to the utilizable or useful power whereas the performance is based on the ratio of utilizable (useful) power to solar power incident on the FPSC. Hypothetically, the present design has considered negligible side wall losses since the base and side walls are subjected to critical insulation thickness design with a minimal power loss to the surroundings. The convectional FPSCs have welded tubes for transporting heat but are less efficient than tubeless ones [1]. The pitfall of FPSC is generation of low exit fluid temperature ($\leq$ 60 ^{o}C). According to Shemelin and Matuska [2], who suggested the following remedies; reduction of natural convection heat transfer in the space between the absorber and the cover by; covering FPSC with multiple glaze or transparent insulation materials (TIM), spreading silica gel along the duct, using lower thermal conductivity working fluids than air or by evacuating the fluid space in accordance to Shire et al. [3], Kessentini et al. [4], Duan [5] and Khorasanizadeh et al. [6]. However, the present work suggests that FPSC cannot stand alone for high temperature application and should be connected to a concentrator, such that it should serves as a preheating unit to a reheating unit (concentrating solar collector); then, its application becomes more lucrative. The present work tends to design a connecting box to be fitted to the exit end of the FPSC, which will allow the absorber of a reheating unit to be fitted into the FPSC to form an integrated system.

Most research works [2, 4, 7–9] have adopted design equations with partial thermal balance, that considers only top loss and ignored other losses; side walls and base, which are not accounted in determining the utilizable heat. Thus, the reported efficiency could be spurious or exaggerated but the present work strictly considers an absolute thermal balance in determining the utilizable heat and will present unexaggerated efficiency and effectiveness of the preheating unit (FPSC).

Based on literature [2, 4, 7, 9], their design of FPSC utilizable or useful power only on the top loss overall transfer coefficient, which neglects other losses because they negated

*Corresponding Author Email: *stephen.nnamchi@kiu.ac.ug* (S. N. Nnamchi)

to carry out thermal balance; in which the present work is championing on, to base the utilizable or useful power on the absolute transfer coefficient instead of the top loss coefficient alone. Obviously, this error could falsify the design efficiency. Thus, thermal balances will be very vital in the design of FPSC [10] as it will draw out all the loss coefficients in computing practical utilizable power and the performance of the FPSC.

Pertinently, the present work will employ gradient method of simulation (characterized by multiple input multiple output) to obtain "n" design primary variables from commensurate thermally formulated independent and temperature sensitive (or functional) design equations; which are pivoted on the component and overall thermal balance on the preheating unit (FPSC), and on the statement of efficiency and effectiveness of the preheating unit. Contrarily, the traditional design approach of single input and output is characterized by disharmony (lack of convergence) among the design variables; hence, result in low performance of the unit. The present work will employ multiple input and multiple out (MIMO) approach to ensure stability or convergence (harmony) among the design variables which engenders high performance of the designed unit.

Conspicuously, very few designs have made the thermal coefficients and the heat transfer fluid (HTF) properties to be temperature sensitive [11–13]. This is vital for direct optimization of the exit fluid temperature, which is an important aspect of this work. Advertently, the fundamental fluid properties (density, viscosity, thermal conductivity, specific heat capacity, thermal conductivity, etc.) will be presented as a function of temperature in this work, which introduces a new and more realistic approach to investigate the thermal efficiency of the preheating unit (FPSC + connecting box) under varying physical conditions.

In computing the utilizable power according to literature [7, 14–17] considered derating the utilizable power with the heat removal factor, 0.723. However, the present work has considered it to be equivalent to the effectiveness of the FPSC, this is incorporated into the present design by developing one of the thermal balance equations on the effectiveness of the unit. Essentially, the current work has based the design formulations on limited assumptions (steady state condition and equality of internal transfer coefficients) to simplify a nonlinear thermal balance equation prior to direct optimization of the exit fluid temperature. Primarily, formulation of the design equations is premium in the design process in order to account for the intricate and peculiar behaviour of the unit.

Exceptionally, the following researchers have employed numerical techniques in the analysis of FPSC [18–20]. But, exact differential technique is deployed in the simulation of FPSC design variables to achieve a better result. Therefore, this work will employ an exact differential to guarantee high performance of the preheating unit in order to eliminate errors due to truncation which are common in the numerical techniques; it is envisaged to enhance the performance of the preheating unit and the design precision generally. Assiduously, the design equations have to be formulated by thermal balance, to stimulate the simulation of the design variables (which are the unknowns in the formulated design equations). Otherwise, the design variables are computed on a single input and single out (SISO) basis, which does not encourage the desired harmony among the design variables and could lead to low performance of the unit.

Appropriately, the dimensions of the preheating unit will be established by meticulous development and incorporation of heat transfer coefficients (the convective and radiative in an enclosed and none enclosed unit configuration) into the thermally formulated design equations for explicit derivation of the exact partial derivatives leading to the simulator matrices and multiple output solutions (which are convergent and optimum) solutions. The output design variables (or dimensions) are germane for producing the detailed engineering drawings prior to fabrication of the preheating unit.

Fundamentally, Bolaji and Abiala [21], Kumar and Mullick [22] articulated the transfer coefficients in the analysis of heat transfer in FPSC, in the same vein. The present work will consider detailed analysis of heat transfer coefficients in formulating thermal losses. Notably, the thermal balance of the unit has to be developed taking into account the tripartite heat transfer such as; conduction, convection and radiation in the individual components of the unit with minimal assumption that could simplify the design equations to amenable solution.

Effectively, the application of low thermal conductivity fluids, silica gel, multiple glaze, honey comb, transparent insulation materials (TIM) for the improvement of the performance of FPSC has been investigated by Shire et al. [3], Kessentini et al. [4], Duan [5]. However, the present work is considering integrating it to a reheating unit as a means of boosting its performance for high temperature requirement via a connecting box. Therefore, a connecting box will be developed which will be able to link the different cross-sections of the preheating unit and a reheating unit together, which is recent innovation by this work in trying to diversify the application of FPSC for extensive drying upon integration with a reheating unit to generate more power to accommodate drying of high moisture foodstuffs and nonfood stuffs.

Strategically, Patil and Deshmukh [8], Ma et al. [23] recommended a practical insulation thickness of 0.06m for FPSC designs but the present work shall implement Rajput [24] method of establishing a critical insulation thickness. The critical lagging thickness is determined for the unit in order to conserve power as much as possible and to increase its efficiency is considered in developing the base thermal loss equation.

Consequently, the present design approach (MIMO) is pivoted on; formulation of temperature sensitive thermal balance equations, simulation of the equations to produce convergent design variables, optimization of the exit fluid temperature and testing the response of the unit to changes in the environmental conditions. Conventionally, the logical steps and procedures to achieve the aforementioned objectives include; materials and method, result presentation and discussion, conclusions and recommendation on the results.

MATERIALS AND METHOD

Uniquely, the design equation is formulated from the first

principle by carrying out component and overall thermal balance on the preheating system and by application of performance equations (effectiveness and efficiency) to build six design equations made up of three thermal (temperatures) and geometric relations (three dimensions of the preheating unit). Moreover, the effects of physical changes such as; inlet or ambient temperature, heat rejection factor, ratio of top to base air velocity on the preheating unit is considered. The simulation is characterized by multiple inputs and multiple outputs, MIMO of six major design output variables appropriate for the design of large systems. It is possible by formulating feasible design equations, which eliminate the error of fixing parameters (single input and single output, SISO). Essentially, the design precision is achieved by Gradient method by seeking the exact partial derivatives of the simulatory matrices, which converge to a practical solution. Then, the convergence of the system of equations will lead to zero degree of freedom (DOF), which implies that no parameter (especially fluid properties) was fixed (but made to be temperature sensitive) during the simulation. The exit fluid temperature is optimized by simple differentiation since the fluid properties are function of temperature. Furthermore, the changes in the physical conditions are simulated on the performance of preheating unit (PPU) to discover their overall effects. Additionally, the computed thermal efficiency and effectiveness of the preheating unit is used to validate the practical and operational data from the designed and fabricated system.

Formulation of design equations

The formulation of the design equations is based on a careful recognition of thermal efficiency, effectiveness, component thermal balance on the glass cover, fluid space and absorber plate, and overall thermal balance around the preheating unit (flat-plate solar collector + connecting box). The design formulation attempts to identify the basic or primary design variables (thermal variables; temperature of the absorber plate, T_p, temperature of the glass cover, T_g, exit temperature of heat transfer fluid, $T_{f,o}$, and the geometric variables; length of the duct, l_d, width of the duct, ω_d and height of the duct, δ_d) and to develop design equations revolving on these variables. Thermal balance on the preheating unit is demonstrated in Figure 1. The function $g_1(W)$ describes the net power generation in the preheating unit as defined in Equation (1):

$$g_1 = Q_{so1,g} - Q_{so1,g-a} - Q_g - Q_p(W);$$

$$\Rightarrow g_1 = \begin{pmatrix} 1-(\rho_g+\tau_g^2\rho_p+\tau_g^2\rho_g\rho_p^2) \\ -(\alpha_g+\tau_g\alpha_g\rho_p+\tau_g\alpha_g\rho_g\rho_p^2) \\ -(\tau_g\alpha_p+\tau_g\alpha_p\rho_g\rho_p+\tau_g\alpha_p\rho_g^2\rho_p^2) \end{pmatrix}(\omega_d l_d)G(W)g_1 \to 0 \quad (1)$$

where $Q_{so1,g}$ *(W)* is the power reaching the surface of the preheating unit (glass cover), $Q_{so1,g-a}$ *(W)* is the power reflected from the glass to the ambient, Q_g *(W)* is the power absorbed by glass, $Q_p(W)$ is the transmitted power absorbed by the absorber plate, ρ_g *(-)* is the reflectance of the glass , τ_g *(-)* is the transmittance of the glass, ρ_p *(-)* is the reflectance of the absorber plate, α_g *(-)* is the absorbance of the glass, α_g *(-)* is the absorbance of the absorber plate and $G(W/m^2)$ is the irradiance reaching the surface of the preheating unit (glass cover).

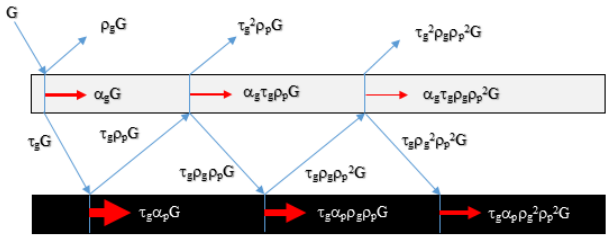

Figure 1. Solar irradiance and thermal flux generation within the preheating unit

Figure 2 illustrates overall steady-state thermal balance around the preheating unit for negligible side wall heat losses. The net power function, g_2 *(W)* in Equation (2) is summed up as follows:

$$g_2 = Q_{so2,g-p} - Q_{cv,g-a} - Q_{r,g-sk} - Q_b - Q_u; Q_{so2,g-p} = \begin{pmatrix} (\alpha_g+\tau_g\alpha_g\rho_p+\tau_g\alpha_g\rho_g\rho_p^2) \\ +(\tau_g\alpha_p+\tau_g\alpha_p\rho_g\rho_p+\tau_g\alpha_p\rho_g^2\rho_p^2) \end{pmatrix} A_{s,g}G(W)\exists g_2 \to 0 \quad (2)$$

where $Q_{cv,g-a}$ *(W)* and $Q_{r,g-sk}$ *(W)* is the rate of heat transfer from the glass surface to the ambient and sky which is defined in Equations (20) and (21), respectively, $A_{s,g} = \omega_d l_d\ (m^2)$ is the surface area of the preheating unit available to $G(W/m^2)$.

The utilizable or useful output power or rate of thermodynamic heat transported, Q_u *(W)* in Equation (3) is defined as follows:

$$Q_u = \dot{m}_a cp_a(T_{f,o} - T_{f,i}) = \rho_a cp_a u_{w,i}(\omega_d\delta_d)(T_{f,o} - T_{f,i})u_{w,i}(\omega_d\delta_d)(1.6843 - 0.0015T_{f,o})\begin{pmatrix} 1010.13412 - \\ 0.03977T_{f,o} \\ +0.000105T_{f,o}^2 \end{pmatrix}(T_{f,o} - 298) \quad (3)$$

where $\dot{m}_a(kg/s)$ is the mass rate of HTF(*f*), cp_a *(J/kgK)* is the specific heat capacity of HTF (air, *a*), $T_{f,i}$ *(K)* is the inlet, *i* temperature of HTF, $T_{f,o}$*(K)* is the outlet, *o* temperature of HTF, $\rho_a\ (kg/m^3)$ is the density of HTF, $u_{w,i}$ *(m/s)* is the velocity of wind, *w or* HTF within the duct, ω_d *(m)* is the width of the duct, *d* or preheating unit and δ_d is the height of the duct.

The rate of heat transfer through the base, Q_b *(W)* is formulated with the aid of Figure 3; where R_i (m^2K/W) is the resistance, δ_i *(m)* is the thickness of fabrication materials, k_i *(W/mK)* is the thermal conductivity of the fabrication materials, *h* (W/m^2K) is the convective heat transfer coefficient, *i={1, 2, 3, 4, 5}≡ {plate(p), plywood(pw1), insulation (ins), plywood (pw2), aluminum cover(m)}.*

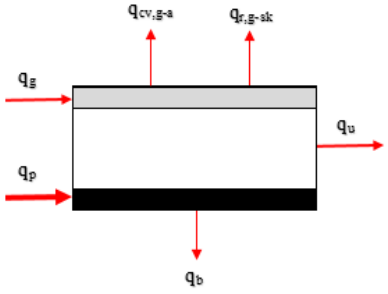

Figure 2. Overall thermal flux around the preheating unit

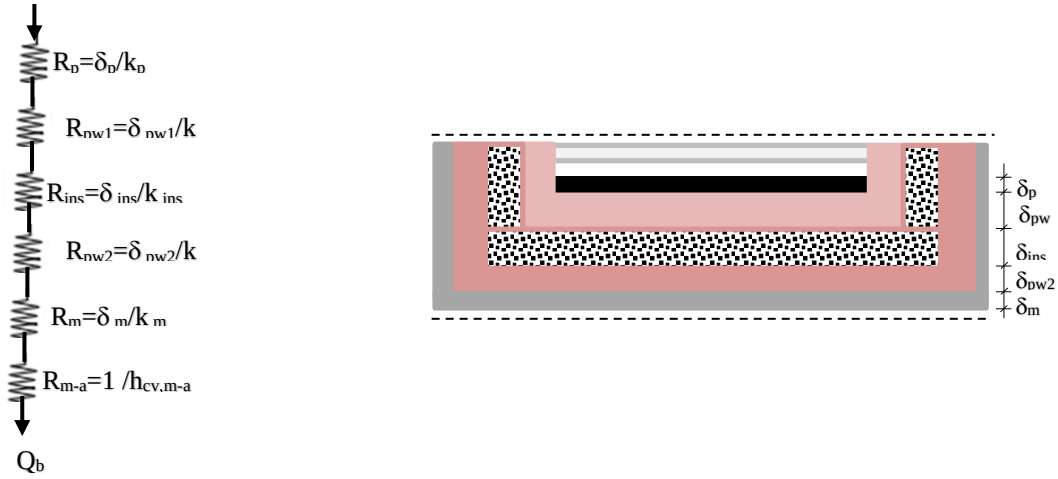

(a) Thermal flux via the base of the preheating unit

(b) Cross-sectional view of the preheating unit

Figure 3. Configuration of the preheating unit (flat-plate solar collector, FPSC), The symbols: *p* = absorber plate, *pw1* = plywood one, *ins* = insulating material, *pw2* = plywood two, *m* = metal cover, *b* = base, *cv* = convective heat transfer, *m-a* = metal cover and ambient (or air), R = resistance, (δ = thickness, *k* = thermal conductivity and *h* = convective heat transfer coefficient

The rate of heat loss through the base, $Q_b(W)$ is expressed in Equation (6) is based on Rajput [24] method for determination of insulation thickness

$$Q_b = U_b A_s (T_p - T_a) = \frac{(\omega_d l_d)(T_p - 298)}{\left(0.178624 + \left(\left(\frac{1}{n} - 1\right)\left(0.178624 + \frac{1}{4.392773(\lambda_{b-t} u_{w,o})^{0.5} l_d^{-0.5}}\right)\right) + \frac{1}{4.392773(\lambda_{b-t} u_{w,o})^{0.5} l_d^{-0.5}}\right)} \quad (6)$$

where $\lambda_{b\text{-}t}$ *(-)* is the base to top wind speed ratio, u_{wo} *(m/s)* is the external wind speed.

An explicit definition of the power loss through the top of the preheating unit is given in Equation (11) as follows:

$$Q_t = \left(\frac{\omega_d l_d (T_{f,o} - 298)}{\frac{1}{h_{r,g-sk} + h_{cv,g-a}} + \frac{h_{cv,p-f} h_{r,p-g} + h_{cv,g-f} h_{r,p-g} + h_{cv,g-f} h_{cv,p-f}}{h_{cv,p-f} + h_{cv,g-f}} + \frac{\delta_g}{k_g}}\right) \quad (11)$$

where h *(W/m²K)* is the heat transfer coefficient, $\delta(m)$ is the thickness of glass (g) and k (W/mK) is the thermal conductivity of the glass. The subscripts; g-sk denotes glass to sky, *cv* is convection, *r* is radiation, *g-a* denotes glass to ambient, *p-f* represents plate to fluid, *p-g* symbolizes plate to glass, *g-f* signifies glass to fluid.

For a considerable variation in the dynamic viscosity of HTF, $h_{cv,p\text{-}f} \neq h_{cv,p\text{-}f,}$ thus, the rate of heat loss through the top of the preheating unit, Q_t *(W)* is formulated as depicted in Figure 4; where *Tp (K)* is the plate temperature, $T_{f,i}(K)$ is the fluid inlet temperature, $T_{f,o}(K)$ is the fluid outlet temperature, $\Delta T_{f\text{-}p}$ *(K)* is the temperature difference between the fluid and plate.

The convective heat transfer coefficient between the absorber plate and HTF, *hcv,p-f (W/m²K)* in Equation (12) is given as follows:

$$h_{cv,p-f} \approx 0.54 \frac{k_a}{l_d} Ra_{l_d}^{\frac{1}{4}};\ 10^4 \leq Ra_{l_d} \leq 10^7 \quad (12)$$

The free convective heat transfer coefficient from the absorber plate to the HTF, *hcv,p-f (W/m²K)* in Equation (13) is empirically defined as follows:

$$h_{cv,p-f} \approx 0.01996 l_d^{-0.25} e^{0.0009375 T_{fo}} \left(\frac{(\cos\phi)\times \begin{pmatrix} -426976.7297 - 655.4854153 T_{fo} + 2.195492077 T_{fo}^2 \\ -0.001293428 T_{fo}^3 + 2.748173\times10^{-7} T_{fo}^4 - 1.18125\times10^{-10} T_{fo}^5 \\ +2865.615635 T_p - 5.216928875 T_{fo} T_p + 0.002771627 T_{fo}^2 T_p \\ -6.20037\times10^{-7} T_{fo}^3 T_p + 2.3625\times10^{-10} T_{fo}^4 T_p \end{pmatrix}}{\begin{pmatrix} 5.53265377\times10^{-5} + 3.37634802\times10^{-7} T_{fo} \\ +4.57651074\times10^{-10} T_{fo}^2 - 1.75614380\times10^{-13} T_{fo}^3 \end{pmatrix}}\right)^{\frac{1}{4}} \quad (13)$$

Similarly, Equation (14) gives a simplified convective heat transfer coefficient, *hcv,f-g (W/m²K)* between the HTF and glass is expressed as follows:

$$h_{cv,f-g} \approx 0.01996 l_d^{-0.25} e^{0.0009375 T_{fo}} \left(\frac{(\cos\phi)\times \begin{pmatrix} 426976.7297 + 655.4854153 T_{fo} - 2.195492077 T_{fo}^2 \\ +0.001293428 T_{fo}^3 - 2.748173\times10^{-7} T_{fo}^4 + 1.18125\times10^{-10} T_{fo}^5 \\ -2865.615635 T_g + 5.216928875 T_{fo} T_g - 0.002771627 T_{fo}^2 T_g \\ +6.20037\times10^{-7} T_{fo}^3 T_g - 2.3625\times10^{-10} T_{fo}^4 T_g \end{pmatrix}}{\begin{pmatrix} 5.53265377\times10^{-5} + 3.37634802\times10^{-7} T_{fo} \\ +4.57651074\times10^{-10} T_{fo}^2 - 1.75614380\times10^{-13} T_{fo}^3 \end{pmatrix}}\right)^{\frac{1}{4}} \quad (14)$$

where φ° is the slope of the FPSC.

The radiative heat transfer coefficient, $h_{r,p-g}(W/m^2K)$ for an enclosure ($F_{p\text{-}g}$ *= 1*, $A_{s,p} = A_{s,g}$) in Equation (15) is written as follows:

$$h_{r,p-g} = \frac{\sigma(T_p^4 - T_g^4)}{\left(\frac{1-\varepsilon_p}{\varepsilon_p} + \frac{1}{F_{p-g}} + \left(\frac{1}{\varepsilon_g} - 1\right)\frac{A_{s,p}}{A_{s,g}}\right)(T_p - T_g)} = h_{r,p-g} = 4.9648\times10^{-8} \frac{(T_p^4 - T_g^4)}{(T_p - T_g)} \quad (W/m^2K) \quad (15)$$

where ε(-) is the emissivity of materials, *F*(-) is the view

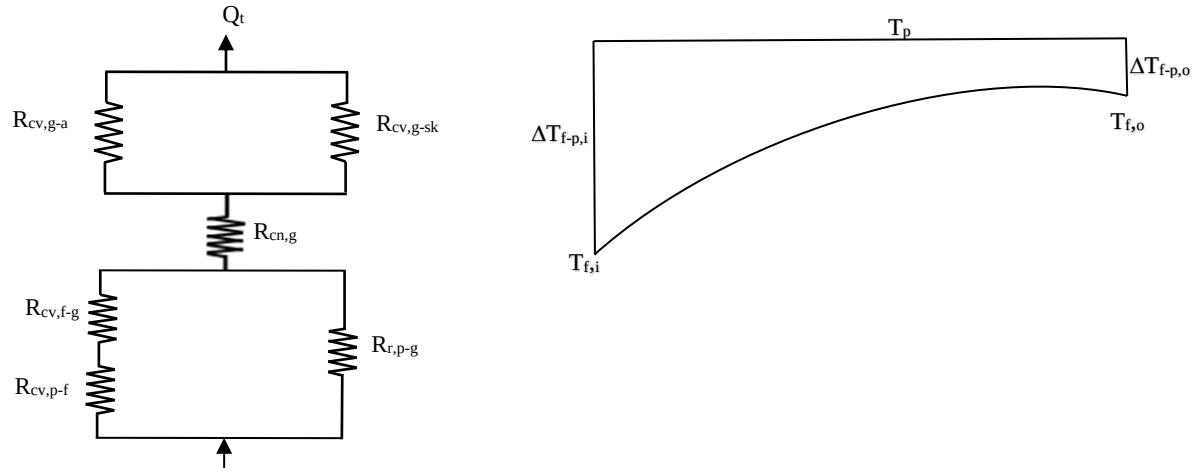

(a) Thermal resistance from the absorber plate to the surface of glass

(b) Heat transfer fluid temperature profile within the preheating unit

Figure 4. Heat transfer fluid temperature distribution within the preheating unit

factor, σ is Stefan constant (5.67×10^{-8} W/m^2K^4) forced convective heat transfer coefficient, $h_{cv,g-a}(W/m^2K)$ between the glass and surrounding (ambient) air is expressed in Equation (16)

$$h_{cv,g-a} = \frac{k_a}{l_d}\left[0.664\,Re_{l_d}^{1/2}\,Pr^{1/3}\right] = \frac{0.664k_a}{l_d}\left[\left(\frac{\rho_a u_{w,t} l_d}{\mu_a}\right)^{1/2}\left(\frac{\mu_a cp_a}{k_a}\right)^{1/3}\right](W/m^2K) \quad (16)$$

For $T_{f,i}$= *298.15(K)*, Equation (16) reduces to Equation (17):

$$h_{cv,g-a} = \frac{4.392773\left(u_{w,o}l_d\right)^{0.5}}{l_d} = 4.392773\left(u_{w,o}^{0.5}l_d^{-0.5}\right)(W/m^2K); \quad \Rightarrow Q_{cv,g-a} = h_{cv,g-a}(\omega_d l_d)\left(T_g - T_a\right)(W) \quad (17)$$

The radiative heat transfer coefficient, h_r, *g-sk (W/m²K)* for a non-enclosure in Equation (18) is given as follows:

$$h_{r,g-sk} = \frac{\varepsilon_g\sigma\left(T_g^4 - T_{sk}^4\right)}{\left(T_g - T_{sk}\right)} = \frac{5.103\times10^{-8}\left(T_g^4 - 6502103756\right)}{\left(T_g - T_{sk}\right)}(W/m^2K); \quad \Rightarrow Q_{r,g-sk} = h_{r,g-sk}(\omega_d l_d)\left(T_g - T_{sk}\right)(W) \quad (18)$$

Considering a thermal component balance on the glaze (glass cover); the unsteady-state thermal balance based on Figure 5 is given in Equation (19)

$$\Rightarrow g_3 = \left(\alpha_g + \tau_g\alpha_g\rho_p + \tau_g\alpha_g\rho_g\rho_p^2\right)(\omega_d l_d)G + (1-y)\begin{pmatrix} h_{cv,p-f}(\omega_d l_d)\left(T_p - 0.5T_{f,o} - 149\right) \\ +h_{r,p-g}(\omega_d l_d)\left(T_p - T_g\right)\end{pmatrix} - h_{cv,g-a}(\omega_d l_d)\left(T_g - 298\right) - h_{r,g-sk}(\omega_d l_d)\left(T_g - T_{sk}\right) = 0(W)\exists g_3 \to 0;\ V_g = A_{s,g}\delta_g(m^3) \quad (19)$$

where *y* $Q_{so3,g}$ *(W)* is the solar irradiance absorbed on the glass cover and y in Figure 5 is the fraction of convective and radiative powers from the absorber plate which are converted to use utilizable power.

According to Nnamchi et al. [25] the sky temperature in Equation (18) is related to the ambient temperature in Equation (20):

$$T_{sk} = 0.0552T_{f,i}^{1.5}(K); \quad (20)$$

Figure 6 depicts a steady state thermal balance within the duct or fluid space which is formulated in Equation (21) as follows:

$$g_4 = y\left(Q_{cv,p-f} + Q_{r,p-g}\right) - Q_{fs-u} = y\left(h_{cv,p-f}(\omega_d l_d)\left(T_p - 0.5T_{f,o} - 149\right) + h_{r,p-g}(\omega_d l_d)\left(T_p - T_g\right)\right) - u_{w,i}(\omega_d\delta_d)\left(1.6843 - 0.0015T_{f,o}\right)\left(1010.13412 - 0.03977T_{f,o} + 0.000105T_{f,o}^2\right)\left(T_{f,o} - 298\right) = 0(W)\exists g_4 \to 0 \quad (21)$$

where Q_{fs-u} *(W)* is the utilizable power transfer from the absorber plate and *y* (-) is the fraction of power utilizable.

Figure 7 illustrates a steady-state thermal balance around the absorber plate whereas Equation (22) gives a mathematical notation of component thermal balance on the absorber plate.

$$Q_{so5,p} - Q_{cv,p-f} - Q_{r,p-g} - Q_b(W) \Rightarrow g_5 = \left(\tau_g\alpha_p + \tau_g\alpha_p\rho_g\rho_p + \tau_g\alpha_p\rho_g^2\rho_p^2\right)(\omega_d l_d)G - \begin{pmatrix} h_{cv,p-f}(\omega_d l_d)\left(T_p - 0.5T_f - 149\right) \\ +h_{r,p-g}(\omega_d l_d)\left(T_p - T_g\right) \\ +U_b(\omega_d l_d)\left(T_p - 298\right)\end{pmatrix}(W)\exists g_5 \to 0 \quad (22)$$

where $h_{cv,p-f}$ *(W)*, $h_{r,p-g}$ *(W/m²K)* and U_b *(W/m²K)* is defined in Equations (13), (14) and (6), respectively. $\tau_g\alpha_p$ is the product of transmissivity of glass and absorptivity of the absorber plate (p) and $Q_{so5,p}$ *(W)* is the transmitted solar irradiance absorbed by the absorber plate.

For effective design of the preheating unit or minimization of heat losses, $Q_t/Q_{u'} = \Psi_{min} < 1$ according to Siebers and Viskanta [7]. Thus, considering an appreciable power gained by the heat transfer fluid against the power lost through the top of the preheating unit such that $\Psi_{design} < \Psi_{min}$ for the preheating unit in Figure 4 results in Equation (23):

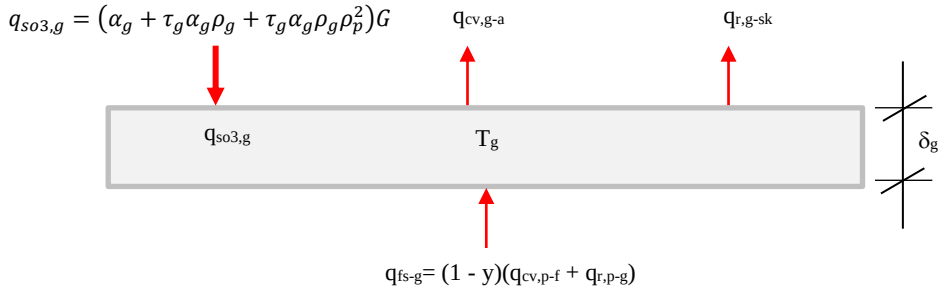

Figure 5. Thermal flux balance around the glass cover

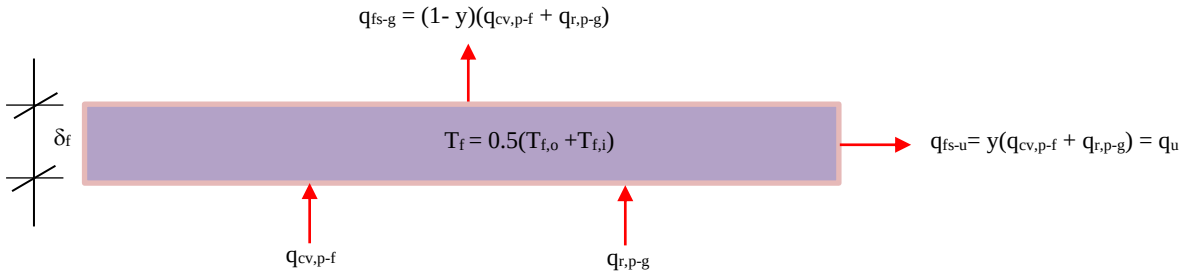

Figure 6. Thermal flux balance within the fluid space

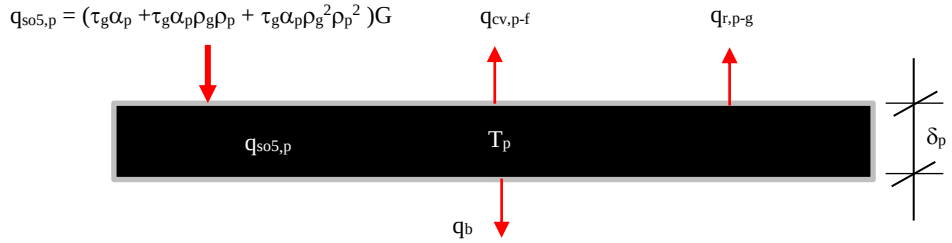

Figure 7. Thermal flux balance around the absorber plate

$$g_6 = Q_t - \Psi Q_u \exists g_6 \to 0$$

$$g_6 = \left(\frac{\omega_d l_d}{\frac{1}{h_{r,g-sk}+h_{cv,g-a}} + \frac{h_{cv,p-f}+h_{cv,f-g}}{h_{cv,p-f}h_{r,p-g}+h_{cv,f-g}h_{r,p-g}+h_{cv,f-g}h_{cv,p-f}} + \frac{\delta_g}{k_g}}\right)\left(\frac{T_{f,o}-298}{ln\left(\frac{T_p-298}{T_p-T_{f,o}}\right)}\right) - \Psi u_{w,i}(\omega_d\delta_d)(1.6843 - 0.0015T_{f,o})(1010.13412 - 0.03977T_{f,o} + 0.000105T_{f,o}^2)(T_{f,o} - 298) = 0(W) \quad (23)$$

where $hcv,p\text{-}f$ (W/m^2K), $h_{cv,f\text{-}g}$ (W/m^2K), $h_{r,p\text{-}g}$ (W/m^2K), $h_{cv,g\text{-}a}$ (W/m^2K) and $h_{r,g\text{-}sk}$ (W/m^2K) is defined Equations (13), (14), (16) and (17), respectively, Ψ (-) is the ratio of top loss to utilizable power.

Determination of the tri-geometric and tri-thermal design variables

Equation (24) represents a gradient method of simulation of thermal system which is applied in the simulation of the preheating unit.

$$\begin{bmatrix} \partial g_1/\partial T_p & \partial g_1/\partial T_g & \partial g_1/\partial T_{f,o} & \partial g_1/\partial l_d & \partial g_1/\partial \omega_d & \partial g_1/\partial \delta_d \\ \partial g_2/\partial T_p & \partial g_2/\partial T_g & \partial g_2/\partial T_{f,o} & \partial g_2/\partial l_d & \partial g_2/\partial \omega_d & \partial g_2/\partial \delta_d \\ \partial g_3/\partial T_p & \partial g_3/\partial T_g & \partial g_3/\partial T_{f,o} & \partial g_3/\partial l_d & \partial g_3/\partial \omega_d & \partial g_3/\partial \delta_d \\ \partial g_4/\partial T_p & \partial g_4/\partial T_g & \partial g_4/\partial T_{f,o} & \partial g_4/\partial l_d & \partial g_4/\partial \omega_d & \partial g_4/\partial \delta_d \\ \partial g_5/\partial T_p & \partial g_5/\partial T_g & \partial g_5/\partial T_{f,o} & \partial g_5/\partial l_d & \partial g_5/\partial \omega_d & \partial g5/\partial \delta_d \\ \partial g_6/\partial T_p & \partial g_6/\partial T_g & \partial g_6/\partial T_{f,o} & \partial g_6/\partial l_d & \partial g_6/\partial \omega_d & \partial g_6/\partial \delta_d \end{bmatrix} \quad (24)$$

$$\begin{bmatrix} \Delta T_p \\ \Delta T_g \\ \Delta T_{f,o} \\ \Delta l_d \\ \Delta \omega_d \\ \Delta \delta_d \end{bmatrix} = \begin{bmatrix} g_1 \\ g_2 \\ g_3 \\ g_4 \\ g_5 \\ g_6 \end{bmatrix}$$

where $g_i(W)$ is the net power balance. The exact partial derivatives or elements of the coefficient matrix in Equation (23) are detailed in the supplementary file.

The future values of the design variables and present values are defined as follows in Equation (25):

$$T_{p,i+1} = T_{p,i} + \Delta T_p;\ T_{g,i+1} = T_{g,i} + \Delta T_g;\ T_{fo,i+1} = T_{fo,i} + \Delta T_{fo};\ l_{d,i+1} = l_{d,i} + \Delta l_d;\ \omega_{d,i+1} = \omega_{d,i} + \Delta\omega_d;\ \delta_{d,i+1} = \delta_{d,i} + \Delta\delta_d;\ \ i = 0,1,2,\cdots,N. \quad (25)$$

The final design variable is established the moment the set convergence criterion ($\zeta = 10^{-3}$ or arbitrarily set value) in Equation (26) is attained:

$$T_{p,i+1} - T_{p,i} \le \zeta;\ T_{g,i+1} - T_{g,i} \le \zeta;\ T_{fo,i+1} - T_{fo,i} \le \zeta;\\ l_{d,i+1} - l_{d,i} \le \zeta;\ \omega_{d,i+1} - \omega_{d,i} \le \zeta;\ \delta_{d,i+1} - \delta_{d,i} \le \zeta;\\ i = 0,1,2,\cdots,N. \quad (26)$$

Optimum design of key the design variables

Considering dominance and equal contribution by natural convection current, then, Equation (23) reduced to Equation (27). Rearranging Equation (26) produces an expression for the number of transfer unit, NTU in Equation (28). Plotting NTU against $T_{f,o}$ *(K)* in Equation (28), fitting the curve with a trend line in Figure 8 and differentiating the equation of the curve with respect to the exit fluid temperature, $T_{f,o}$ *(K)* gives the optimum value of the exit fluid temperature, $T^*_{f,o}$ *(K)* as shown in Figure 8.

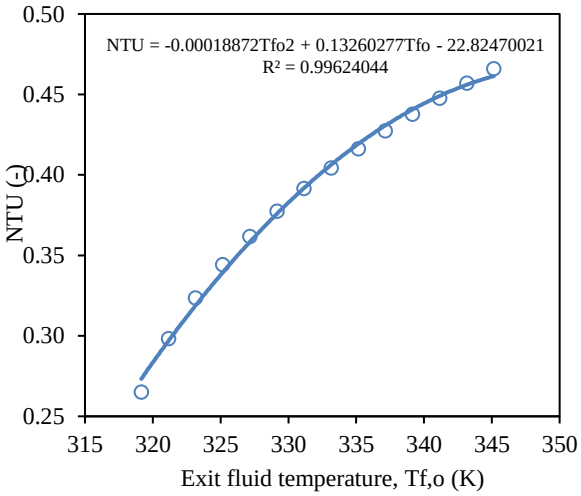

Figure 8. Optimum exit fluid temperature at inlet fluid temperature of 298 K

$$g_6 = 0.00998\omega_d l_d^{0.75} e^{0.0009375T_{fo}} \left(\frac{(\cos\phi)\times \begin{pmatrix} 426976.7297+655.4854153T_{fo}-2.195492077T_{fo}^2 \\ +0.001293428T_{fo}^3-2.748173\times10^{-7}T_{fo}^4+1.18125\times10^{-10}T_{fo}^5 \\ -2865.615635T_g+5.216928875T_{fo}T_g-0.002771627T_{fo}^2T_g \\ +6.20037\times10^{-7}T_{fo}^3T_g-2.3625\times10^{-10}T_{fo}^4T_g \end{pmatrix}}{\begin{pmatrix} 5.53265377\times10^{-5}+3.37634802\times10^{-7}T_{fo} \\ +4.57651074\times10^{-10}T_{fo}^2-1.75614380\times10^{-13}T_{fo}^3 \end{pmatrix}} \right)^{\frac{1}{4}} \left(\frac{1}{ln\left(\frac{T_p-298}{T_p-T_{f,o}}\right)} \right) - \Psi u_{w,i}(\omega_d\delta_d)\left(1.6843 - 0.0015T_{f,o}\right)\left(1010.13412 - 0.03977T_{f,o} + 0.000105T_{f,o}^2\right)(W) \quad (27)$$

$$NTU = \frac{0.00998\omega_d l_d^{0.75} e^{0.0009375T_{fo}} \left(\frac{(\cos\phi)\times \begin{pmatrix} 426976.7297+655.4854153T_{fo}-2.195492077T_{fo}^2 \\ +0.001293428T_{fo}^3-2.748173\times10^{-7}T_{fo}^4+1.18125\times10^{-10}T_{fo}^5 \\ -2865.615635T_g+5.216928875T_{fo}T_g-0.002771627T_{fo}^2T_g \\ +6.20037\times10^{-7}T_{fo}^3T_g-2.3625\times10^{-10}T_{fo}^4T_g \end{pmatrix}}{\begin{pmatrix} 5.53265377\times10^{-5}+3.37634802\times10^{-7}T_{fo} \\ +4.57651074\times10^{-10}T_{fo}^2-1.75614380\times10^{-13}T_{fo}^3 \end{pmatrix}} \right)^{\frac{1}{4}}}{\Psi u_{w,i}(\omega_d\delta_d)\left(1.6843-0.0015T_{f,o}\right)\left(1010.13412-0.03977T_{f,o}+0.000105T_{f,o}^2\right)}(-) \quad (28)$$

Simulation of exit fluid temperature with respect to physical conditions

Simulation of the outlet temperature of HTF becomes necessary in order to have overview of the effect of the physical conditions; the solar irradiance, mass flowrate of heat transfer fluid and ambient conditions on the performance of the preheating unit.

RESULTS AND DISCUSSION

This section contains a sequential presentation of figures and tables of results. A total of seventeen figures were generated in the design, under four categories; Figures 1 to 7 give the illustration of the design formulation and thermal balance. The second category; Optimum exit fluid temperature at the inlet fluid temperature of 298 K in Figure 8, the third category; Figures 9 to 11 contain the results of simulation of physical conditions on the preheating unit and fifth category; Figures 12 and 13 contain the isometric and detailed engineering drawings, respectively for the fabrication of the preheating unit.

Subsequently, the series of table of input data and results are; Table 1 which provides the input data to the design equations (Equations (1) to (28)), Table 2 furnishes the preheating unit material specification and properties, Table 3 depicts the simulation results for the key design variables and Table 4 holds the design evaluated parameters.

Results presentation

Table 1 avails the input data for the design of the preheating unit; the optical properties, the dimensions of the preheating unit, temperatures, the wind speed and its slope. The data are very important for the initiation of the simulation and formation of simulatory matrices. Table 2 unveils the materials for the fabrication of the preheating unit and their specifications; glass cover, absorber plate (mild steel sheet), insulating material (pulverized saw dust) and wrapping (cover) material (aluminum coil), these information were used to compute power losses; through the top, side walls and the base. Table 4 contains the evaluated design results whereas Table 3 shows the simulation result of the design; the thermal design variables and geometric design variables and the net value of the design equations (net power). At the

seventh iteration, the design variables were no longer changing and besides, the net power functions were all tending to zero indicating that convergence or harmony among the design variables has been attained. Of course, the values of the design variables at the seventh iteration were used to analyse the preheating unit performance; the efficiency and effectiveness of the preheating unit and to fathom the effect of changes of physical conditions on the preheating unit and its responses.

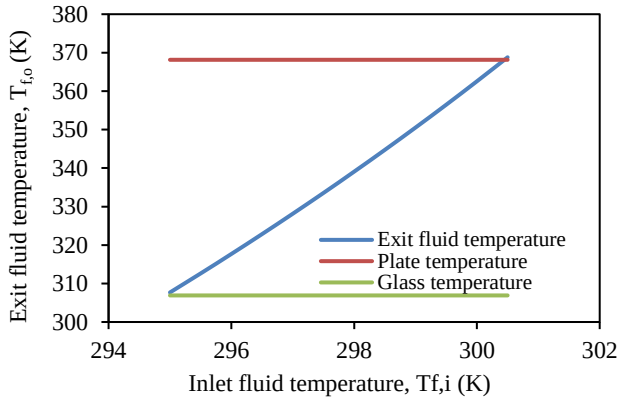

Figure 9. Practical inlet fluid temperature for the design of the preheating unit

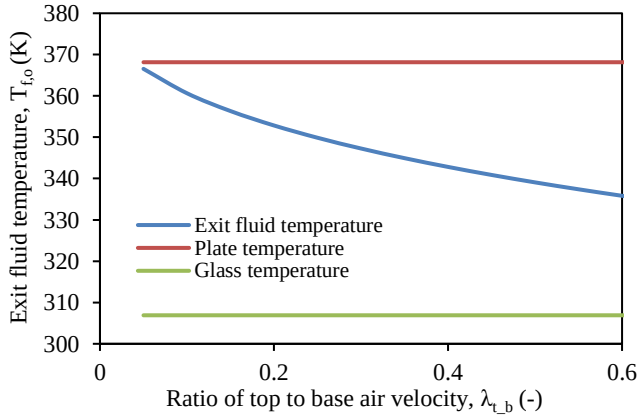

Figure 10. Practical ratio of top to base air velocity for the design of the preheating unit

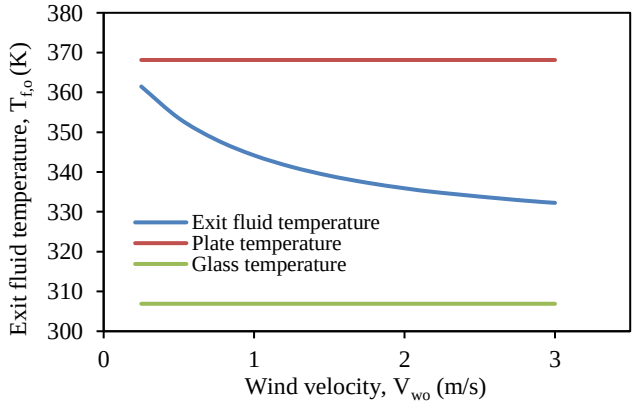

Figure 11. Practical wind velocity for the design of the preheating unit

Discussion

The output of the simulation, the design variables; T_p *(K)*, T_g *(K)*, $T_{f,o}$ *(K)*, l_d *(m)*, ω_d *(m)* and δ_d *(m)* (m) are 368.1, 306.9, 339.1, 2.011,1.005 and 0.040, respectively in Table 4.

The design exit fluid temperature ($T_{f,o}$) is in good agreement with the reported data by Shemelin and Matuska [2]. Whereas the net power functions; $g_1(W)$, $g_2(W)$, $g_3(W)$, $g_4(W)$, $g_5(W)$, and $g_6(W)$, are 0.0017→0, 0.0015→0, -0.0534→0, 0.0348→0, 0.0081→0 and 0.0043→0, respectively for the design equations; Equations (1), (2), (19), (21), (22) and (23), respectively, are all tending to zero, which substantiate the fact that the simulatory matrices; the coefficient matrix of Equation (23) is nonsingular matrices or invertible matrix, which guarantees that the product of the inverse matrix with the column matrix yielded a definite solution (the change in design variables in Equation (25)). Then, the change in the variables is added to the previous design variables to obtain new values of the design variables in Equation (26).

The iteration was repeated until a convergence was attained. The last iteration values form the final design variables, which satisfied the convergence criterion. The final temperatures; T_p (K), T_g (K), $T_{f,o}$ (K) are useful for computation of utilizable power and the performance parameters; the efficiency and effectiveness of the preheating unit.

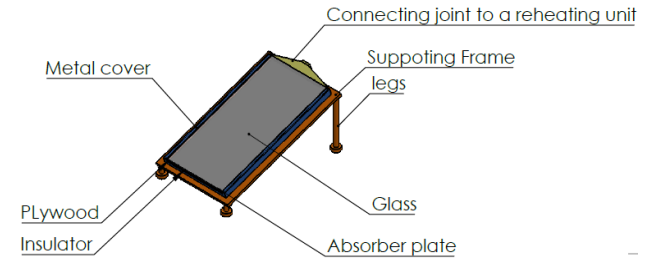

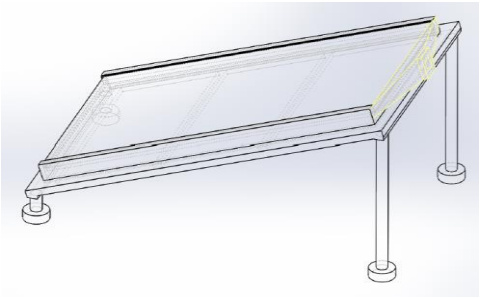

(12a) Front view

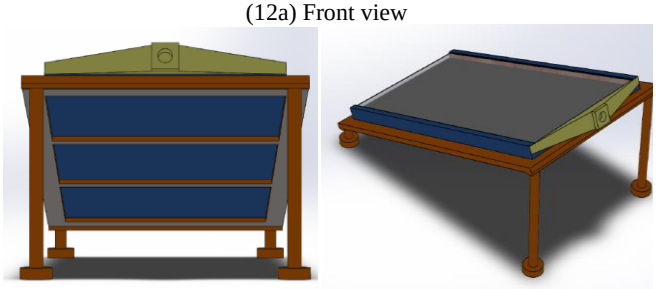

(12b) Rear view

Figure 12. Isometric drawing of the preheating unit

The optimum exit fluid temperature was obtained from Equation (28), which yielded the optimum mass flowrate (0.0228 kg/s) of the heat transfer fluid and utilizable power (1224.63 W). The optimum design efficiency (0.76) was based on the optimum utilizable power (1224.63 W), which gave rise to the upper limit of the design efficiency (0.76), whereas the utilizable power calculated from the simulation, yield the design efficiency (0.64) corresponding to lower limit of the design efficiency (0.64), which is thermodynamic acceptable [24]. Correspondingly, the upper and lower limits of the NTU (0.47) were computed and used to compute the optimum effectiveness (0.40) for the preheating unit as presented in Table 4 , which compared well with the literature result 10. The soundness of the design and fabrication will be revealed by the operational performance of the preheating unit while loaded and unloaded. However, that will be actualized in the next paper, since this paper has been over loaded with the art of design.

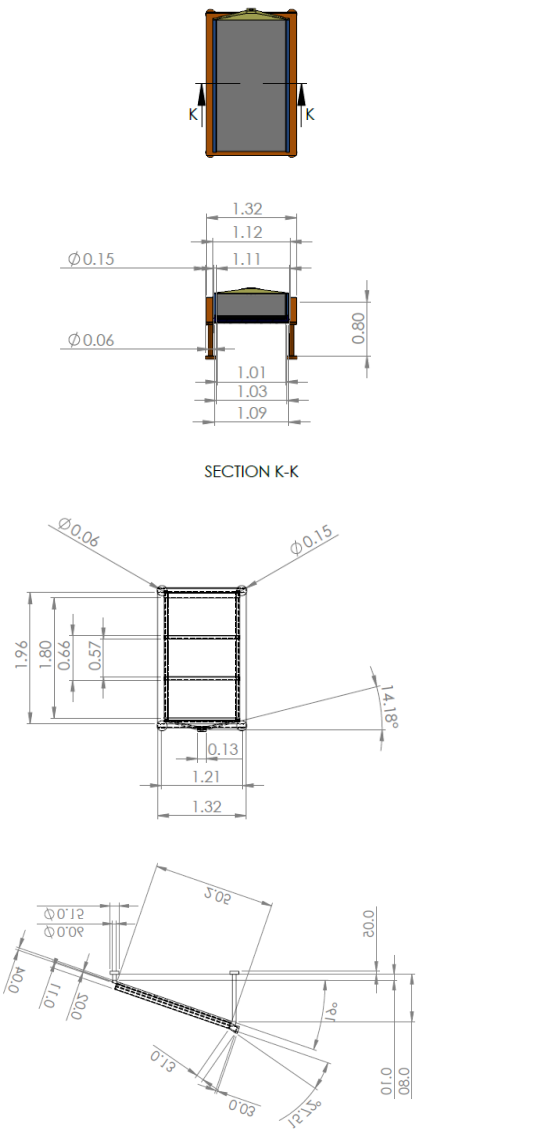

(13a) Preating unit

(13b) Connecting box

Figure 13. Detailed drawing of the Preheating unit and connecting box

TABLE 1. Input data to the design equations

S#	Definition	Symbol	Unit	Value
1.	The absorbance of glass	α_g	(-)	0.05
2.	The reflectance of glass	ρ_g	(-)	0.10
3.	The transmittance of glass	τ_g	(-)	0.85
4.	The absorbance of absorber plate	α	(-)	0.95
5.	The reflectance of absorber plate	ρ_p	(-)	0.05
6.	The transmittance of absorber plate	τ_p	(-)	0.00
7.	The ratio of top to base velocity	$\lambda_{b\text{-}t}$	(-)	0.50
8.	The fraction of power lost thru the base	n	(-)	0.30
9.	The fraction of power utilizable	y	(-)	0.82
10.	The ratio of top loss to utilizable power	Ψ	(-)	0.41
11.	The initial temperature of the plate	T_{p0}	(K)	368.15
12.	The initial temperature of the glass	T_{g0}	(K)	306.9
13.	The initial exit fluid temperature	T_{o0}	(K)	339.15
14.	The initial length of the duct	l_{d0}	(m)	2.010
15.	The initial width of the duct	ω_{d0}	(m)	1.005
16.	The initial height of the duct	δ_{d0}	(m)	0.040
17.	The solar irradiance reaching the preheater	G	(W/m^2)	800
18.	The inlet fluid temperature	T_{fi}	(K)	298
19.	The sky temperature	T_{sk}	(K)	368.15
20.	The slope angle of the preheater	φ	(degree)	19
21.	The wind velocity	$u_{w,O}$	(m/s)	1.5

Figures 9 to 11 show the response of the preheating unit when perturbed with the change in the physical conditions. Specifically, Figure 11 portrays that the inlet temperature of the heat transfer fluid should not exceed 300K, because above 300 K, the exit fluid temperature becomes insensible (attains maximum temperature), this information is also vital for generating constraint equation for comprehensive optimization of the preheating unit. Figure 10 unleashes another optimization constraint equation by limiting the ratio of top to base air velocity to 0.05, further reduction in this parameter does cause any rise in the fluid temperature below 0.05. Figure 11 produces another design constraint equation, heat transfer fluid natural velocity below 0.5 (m/s) does not cause any further rise in the exit fluid temperature. Thus, the fluid velocity should not be retarded below 0.5 (m/s) because it will not cause any significant change in the exit fluid temperature. Consequently, Figures 9 to 11 have yield constraint equations for a holistic optimization of the preheating unit in advance.

Detailed drawings

Figures 12 and 13 present the isometric and detailed drawings of the preheating unit, respectively. The dimensions thereof are obtained from Table 4 (simulation output). Figure 13a gives the detailed drawing of the plan and end view of the preheating unit, which facilitates its fabrication whereas Figure 13b gives the detailed drawing of the connecting box, which will be used to connect the preheating unit to the reheating unit for the envisaged optimum use in drying highly moisturized agricultural foodstuffs or other nonedible materials like timbers.

TABLE 2. Preheating unit material specification and properties

S#	Definition	Symbol	Unit	Value
1.	Glass thickness	δ_g	(m)	0.003
2.	Absorber plate thickness	δ_p	(m)	0.001
3.	Plywood thickness	$\delta_{pw} = \delta_{pw1} = \delta_{pw2}$	(m)	0.0125
4.	Insulator thickness	δ_{ins}	(m)	0.0295
5.	Wrapping material (aluminum coil) thickness	δ_m	(m)	0.005
6.	Glass density	ρ_g	(kg/m^3)	2500
7.	Absorber plate density (mild steel sheet)	ρ_p	(kg/m^3)	7860
8.	Plywood density	$\rho_{pw} = \rho_{pw1} = \rho_{pw2}$	(kg/m^3)	575
9.	Insulator density	ρ_{ins}	(kg/m^3)	210
10.	Cover material (aluminum coil) density	ρ_m	(kg/m^3)	2700
11.	Glass conductivity	k_g	(W/mK)	1.1
12.	Absorber plate conductivity	k_p	(W/mK)	36.04
13.	Plywood conductivity	$k_{pw} = k_{pw1} = k_{pw2}$	(W/mK)	0.14
14.	Insulator conductivity	k_{ins}	(W/mK)	0.14
15.	Cover material (aluminum coil) conductivity	k_m	(W/mK)	205
16.	Mild steel density	ρ_s	(kg/m^3)	7860
17.	Mild steel compressive strength	τ_s	(MPa)	150

TABLE 3. Simulation of the key design variables

i	Temperature			Dimension			Function					
	T_p (K)	T_g (K)	$T_{f,o}$ (K)	l_d (m)	ω_d (m)	δ_d (m)	g_1 (W)	g_2 (W)	g_3 (W)	g_4 (W)	g_5 (W)	g_6 (W)
0	368.1	307.8	314.7	2.016	1.002	0.071	0.0017	40.6484	-1.8619	76.6460	-34.2406	78.7615
1	368.0	307.3	328.3	2.014	1.003	0.051	0.0017	5.5900	-1.6829	19.4924	-12.2526	28.2586
2	368.1	307.1	334.8	2.013	1.004	0.044	0.0017	0.5805	-1.1481	5.8063	-4.0946	10.1560
3	368.1	307.0	337.6	2.012	1.004	0.042	0.0017	0.0150	-0.6826	1.9721	-1.2874	3.6743
4	368.1	306.9	338.6	2.012	1.004	0.041	0.0017	-0.0168	-0.3766	0.7217	-0.3740	1.3488
5	368.1	306.9	338.9	2.012	1.004	0.040	0.0017	-0.0064	-0.1992	0.2738	-0.0929	0.4971
6	368.1	306.9	339.1	2.011	1.004	0.040	0.0017	-0.0004	-0.1031	0.1036	-0.0127	0.1630
7	368.1	306.9	339.1	2.011	1.005	0.040	0.0017	0.0015	-0.0534	0.0348	0.0081	0.0043

TABLE 4. Evaluated design results

S#	Parameter	Symbol	Unit	Values
1.	Number of transfer unit	NTU	(-)	0.4700
2.	Optimum mass flowrate	$\dot{m}$	(kg/s)	0.0228
3.	Optimum utilizable power	Q_u^*	(kW)	1.2250
4.	Optimum thermal efficiency	η_{th}^*	$(-)$	0.7600
5.	Design efficiency	η_{th}	$(-)$	0.6400
6.	Optimum exit fluid temperature	$T_{f,out}^*$	(K)	351.30

CONCLUSIONS

The innovative design of the preheating unit (FPSC) has been accomplished by formulating thermal balance equations on its components; the glass cover, the fluid space, the absorber plate and overall thermal balance, and the thermal balance pivoted on the performance yardsticks; the effectiveness and efficiency of the preheating unit. The design was characterized by six unknown design variables; made up of three geometric variables; the length, width and height of the duct of the preheating unit and three thermal variables; the absorber, working fluid and glass cover temperatures. These variables were established by setting up simulatory matrices, whose elements were obtained by exact partial derivatives of six independently formulated designs equation with respect to the design variables. The convergent values of the simulatory matrices served as the design values for the six key design variables; T_p *(K)*, T_g *(K)*, $T_{f,o}$ *(K)*, l_d *(m)*, ω_d *(m)* and δ_d *(m)* with the numerical values: 368.1, 306.9, 339.1, 2.011,1.005 and 0.040, respectively summarized in Table 4.

The optimum values and performance of the preheating unit were established by differentiating a function of Number of transfer units (*NTU*) with respect to the exit fluid temperature to yield the maximum; exit fluid temperature, $T_{f,o}$ (351.3 K) and *NTU* (0.47), which gave rise to the computation of pragmatic and optimum; fluid mass flowrate (0.0228 kg/s), efficiency (0.76) and effectiveness (0.40) of the preheating unit and these results are true of a device exhibiting an irreversible thermodynamic principle. Thus, the performance results are quite consistent with the operational yardsticks.

The climax of the design is the introduction of connecting box, which is meant to add value to the application of the preheating unit (FPSC + connecting box) in handling high thermal duty operations requiring temperature above 150 ^{o}C by serving as a preheating unit, that raises the temperature of the working fluid up to 78 ^{o}C for the reheating unit, that is capable of concentrating the exit fluid temperature > 150 ^{o}C for drying of highly moisturized agricultural products ($\geq$ 0.80 kg_{water}/kg_{ds}) and other allied products.

Thermodynamically, the preheating unit serves as a tailing unit and the reheating unit serves as a topping unit in forming an integrated system. Thus, this design, will enhance the drying of wide range of agricultural products, with availability of large scale bin. The innovative application of preheating unit by addition of connecting box, has made the application of FPSC to be more lucrative against using it as a standalone device, which cannot produce high temperature required for heavy duty thermal drying as opined by Shemelin and Matuska [2].

SUPPLEMENTARY MATERIALS

The supplementary material contains the partial derivatives or elements of the coefficient matrix in Equation (23). The step by step differentiation that led to each of the thirty-six (36) partial derivatives, which form the simulatory matrices is carefully presented for reader comprehension and scrutiny. Also, the mathematical function of the heat transfer fluid properties is embed in the supplementary material. The supplementary file can be accessed via the following link: http://www.ijee.net/jufile?ar_sfile=1029931

REFERENCES

1. Tamimi, A., 1986. Analysis and design of a novel flat plate solar collector. International Communications in Heat and Mass Transfer, 13(6): 651-657.
2. Shemelin, V. and Matuska, T., 2017. Detailed modeling of flat plate solar collector with vacuum glazing. International Journal of Photoenergy, 2017: 1-9.
3. Shire, G.S.F., Moss, R.W., Henshall, P., Arya, F., Eames, P.C. and Hyde, T., 2016. Development of an efficient low-and medium-temperature vacuum flat-plate solar thermal collector. In: Renewable Energy in the Service of Mankind Vol II. Springer, Cham. pp. 859-866.
4. Kessentini, H., Castro, J., Capdevila, R. and Oliva, A., 2014. Development of flat plate collector with plastic transparent insulation and low-cost overheating protection system. Applied Energy, 133: 206-223.
5. Duan, R., 2012. The efficiency of new solar flat-plate collector. In: Advanced Materials Research (Vol. 347). Trans Tech Publications Ltd., pp. 1337-1341.
6. Khorasanizadeh, H., Aghaei, A., Ehteram, H., Dehghani Yazdeli, R. and Hataminasar, N., 2014. Attaining optimum tilts of flat solar surfaces utilizing measured solar data: case study for Ilam, Iran. Iranian (Iranica) Journal of Energy and Environment, 5(3): 224-232.
7. Siebers, D.L. and Viskanta, R., 1979. Thermal analysis of some flat-plate solar collector designs for improving performance. Journal of Energy, 3(1): 8-15.
8. Patil, P.P. and Deshmukh, D.S., 2015. Design considerations for flat plate solar water heater system. International Journal of Science, Spirituality, Business and Technology, 3(2): 21-25.
9. Bakari, R., Minja, R.J. and Njau, K.N., 2014. Effect of glass thickness on performance of flat plate solar collectors for fruits drying. Journal of Energy, 2014: 1-8.
10. Stoecker, W.F., 1980. Design of thermal systems. McGraw Hill Book Company.
11. Nnamchi, S.N., Nnamchi, O.A., Sangotayo, E.O., Mundu, M.M. and Edosa, O.O., 2019. Design and fabrication of insulation testing rig. Indian Journal of Engineering, 16: 60-79.
12. Nnamchi, S.N., Nnamchi, O.A., Odebiyi, O.S., Edosa, O.O. and Wanazusi, T., 2019. Experimental verification of suitability of insulation testing rig in determining thermophysical properties of insulating materials. Cogent Engineering, 6(1): 1-32.
13. Nnamchi, S.N., Nnamchi, O.A., Martins Onyekwelu Onuorah, E.O. and Sangotayo, V.G., 2019. Modelling and Simulation of Heat Transfer through the Finned Hollow Cylindrical Surfaces of an Insulation Testing Rig. World Journal of Modelling and Simulation, 15(3): 243-261.
14. Kalogirou, S.A., 2013. Solar energy engineering: processes and systems. Academic Press.
15. Rosli, M.A.M., Misha, S., Sopian, K., Mat, S., Sulaiman, M.Y. and Salleh, E., 2014. Parametric analysis on heat removal factor for a flat plate solar collector of serpentine tube. World Applied Sciences Journal, 29(2): 184-187.
16. Malvi, C.S., Gupta, A., Gaur, M.K., Crook, R. and Dixon-Hardy, D.W., 2017. Experimental investigation of heat removal factor in solar flat plate collector for various flow configurations. International Journal of Green Energy, 14(4): 442-448.
17. Montoya-Márquez, O. and Flores-Prieto, J.J., 2018. Heat removal factor in flat plate solar collectors: indoor test method. Energies, 11(10): 1-12.
18. Ullah, F., Khattak, M.K., Kang, M., Li, N., Yang, J. and Wang, X., 2017. Numerical simulation on thermal performance of flat plate solar collector with double glass covers. Journal of Applied Sciences, 17(10): 502-510.

19. Ekramian, E., Etemad, S.G. and Haghshenasfard, M., 2014. Numerical analysis of heat transfer performance of flat plate solar collectors. Journal of Fluid Flow, Heat and Mass Transfer, 1: 38-42.
20. Kazeminejad, H., 2002. Numerical analysis of two dimensional parallel flow flat-plate solar collector. Renewable Energy, 26(2): 309-323.
21. Bolaji, B.O. and Abiala, I.O., 2012. Theoretical and Experimental Analyses of Heat Transfer in a Flat-Plate Solar Collector. Walailak Journal of Science and Technology, 9(3): 239-248.
22. Kumar, S. and Mullick, S.C., 2010. Wind heat transfer coefficient in solar collectors in outdoor conditions. Solar Energy, 84(6): 956-963.
23. Ma, J., Wang, H., Wang, Y., Sun, W. and Ji, J., 2015. Performance Investigation and Structure Optimization of a Flat Dual-Function Solar Collector. International Journal of Photoenergy, 2015: 1-11.
24. Rajput, R.K., 2009. Engineering thermodynamics: A computer approach (si units version). Jones & Bartlett Publishers.
25. Nnamchi, S.N., Sanya, O.D., Zaina, K. and Gabriel, V., 2018. Development of dynamic thermal input models for simulation of photovoltaic generators. International Journal of Ambient Energy, 1-13. https://doi.org/10.1080/01430750.2018.1517676

Persian Abstract

DOI: 10.5829/ijee.2020.11.02.02

چکیده

طراحی یک کلکتور خورشیدی با صفحه صاف (FSPC) با استفاده از تکنیک طراحی ورودی چند خروجی مختلف (MIMO) انجام می‌شود. متغیرهای طراحی (دمای جاذب، سیال و شیشه؛ طول، عرض، ارتفاع (FPSC)) متغیرهای ناشناخته در معادلات موازنه حرارتی متناسب بر اساس موازنه گرمایی اجزا، کلی و معیاری بر FPSC، بودند. سپس، ماتریس شبیه‌سازی شامل ضریب و ماتریس ستون توابع طراحی تنظیم شد. عناصر ماتریس ضریب، با توجه به متغیرهای طراحی، مشتقات جزئی از توابع طراحی بودند. علاوه بر این ضریب انتقال حرارت همرفتی و تابشی تابعی از متغیرهای طراحی بودند. مقادیر اولیه متغیرهای طراحی (به ترتیب ۳۰۷ K، ۳۳۴/۵ K، ۳۶۸ K، ۲ m، ۱ m، و ۰/۰۴۵ m) تعیین شد، در هفتمین تکرار متغیرهای خروجی طراحی (به ترتیب ۳۰۶/۹ K، ۳۳۹/۱۵ K، ۳۶۸/۱ K، ۲/۰۱ m، ۱/۰۰۵ m، و ۰/۰۴ m) به عنوان توابع طراحی ۰ با تغییر ناچیز در متغیرهای طراحی ادغام شدند. نتایج خروجی برای شبیه‌سازی FPSC، برای ردیابی پاسخ آن به تغییرات در شرایط بدنی مورد استفاده قرار گرفت، تحریک برخی محدودیت‌ها در طراحی FPSC را نشان داد، که اطلاعات حیاتی برای بهینه‌سازی کلی FPSC است. معیارهای طراحی؛ راندمان حرارتی (۰/۷۶) و اثربخشی (۰/۴۰) کاملاً عملی است. این نتایج نشان می‌دهد که تکنیک MIMO به طراحی سیستم حرارتی به عنوان همگرایی بین متغیرهای طراحی مؤثر است. علاوه بر این، MIMO تمام افت‌های حرارتی را به جای اینکه معیارهای اصلی را روی ضریب انتقال کلی افت بالا بگذارد، در نظر گرفت و بدین ترتیب جدارهای جانبی و اتلافات اساسی را نادیده گرفت. علاوه بر این، ظهور جعبه اتصال، واحد گرمایش قبل از خشک شدن دمای بالا (< ۱۵۰ درجه سانتی‌گراد) را برای ادغام با واحد گرمایش آماده می‌کند.